Preprints of the 19th World Congress
The International Federation of Automatic Control
Cape Town, South Africa. August 24-29, 2014

Diagnosis of PEM fuel cell stack based on magnetic fields measurements

T. Hamaz*,*. C. Cadet*, F. Druart**, G. Cauffet*****

*Univ. Grenoble Alpes, GIPSA Lab, F-38000 Grenoble, France - CNRS, GIPSA Lab, F-38000 Grenoble, France (e-mail: tahar.hamaz @gipsa-lab.grenoble-inp.fr, catherine.cadet@gipsa-lab.grenoble-inp.fr).
** Univ. Grenoble Alpes Savoie, LEPMI, F-38000 Grenoble, France - CNRS, LEPMI, F-38000 Grenoble, France (e-mail:florence.druart@lepmi.grenoble-inp.fr)
*** Univ. Grenoble Alpes, G2Elab, F-38000 Grenoble, France - CNRS, G2Elab, F-38000 Grenoble, France (e-mail: gilles.cauffet@g2elab.grenoble-inp.fr)

Abstract: Non-uniform current density distribution in PEM fuel cell results in local over-heating, accelerated ageing, and lower power output. This paper proposes a diagnosis approach for PEM fuel cell system based on monitoring the current density distribution inside the stack. A magnetic sensor network has been used to provide an image of the current density distribution. The diagnosis method has three steps: residuals generation, residual analysis to obtain symptoms and decision by classifying these symptoms. The proposed approach has been applied on virtual measurements and validated on experimental measurements under performance degradation due to long term functioning of the PEM fuel cell stack and under low air stoichiometric ratio due to an actuator fault. Results show that the proposed method is a remarkable tool for diagnosis and taking compensatory actions.

Keywords: PEM Fuel Cells, Magnetic fields, Fault diagnosis, Residual analysis, Pattern recognition

1. INTRODUCTION

Polymer Electrolyte Membrane Fuel Cells (PEMFC) appear as a promising alternative to the existing power converters. However, they still suffer from a low reliability and a short lifetime that is why many investigations on durability and degradation issues in PEMFC have been done (Borup *et al.*, 2007). Many papers have shown that main causes of short life and performance degradation are poor water management (Schmittinger *et al.*, 2008). Excess water in a PEM fuel cell may induce water flooding and lack of water drying out of the PEM fuel cell, both resulting in a significant loss of stack performances. In both cases, a drop in the stack voltage is the first indicator of performance degradation.

In the fuel cell stack, several methods using global measurements have been established for the detection of water flooding and membrane drying. (Yousfi Steiner *et al.*, 2010) used a black-box model based on neuron model to diagnosis flooding. (Rubio *et al.*, 2007) showed that the voltage variations induced by a current step were particularly sensitive to water content in a fuel cell. (Görgün *et al.*, 2005) used an approach that requires the measurement of the voltage, current, temperature, total pressure at the cathode and anode to estimate water content of the membrane.

In the auxiliary components, (De Lira *et al.*, 2010) has detected a set of commons possible fault of the sensors based on a LPV interval observer. (Aitouche *et al.*, 2011) has used an extended parity space approach to detect and isolate actuator and sensor faults. However, these sensors faults will induce change in the operating conditions leading to a change in the operation mode of the stack. In all these works, the flooding and drying out of the fuel cell stack are induced by changing deliberately an operating condition. These methods give averaged information on the global state of the fuel cell but do not provide information on the local state inside the fuel cell stack.

(Chikahissa *et al.*, 2009) showed that there were good correlations among the distributions of current density, temperature and water amounts in the stack. The measurement of these physical indicators, and more especially the current density distribution, has been employed as a diagnostic tool to estimate the state of operation in an operating fuel cell. Non-uniform current distribution in PEMFC results in local over-heating, accelerated ageing, and lower power output.

This paper proposes a method allowing the detection and isolation of faults based on monitoring the current density distribution and avoiding the difficulties of inverse problems (Hauer *et al.*, 2005). The method not only provides fault signatures but also gives local information about current density distribution which allows taking compensatory actions to restore uniform current density distribution.

The method compares the real behaviour of the system obtained by means of a magnetic sensor network with diagnostic baselines characterizing the abnormal behaviour of the system. The baselines are calculated using the Biot-Savart equation which gives the relation between the magnetic field and the current density distribution. Decision is obtained by means of residuals analysis. Classes are generated thanks to computed symptoms. The generated classes enable the detection and isolation of faults resulting from changes in the current density distribution.

This paper is organized as follows: first, the magnetic sensors network, the Biot-Savart equation and the diagnosis method are introduced in section 2. In section 3, results using experimental measurements are presented and discussed.

2. MATERIAL AND METHOD

2.1 Material

The polymer electrolyte membrane fuel cells PEMFC convert the chemical energy stored in hydrogen fuel directly and efficiently to electrical energy with water as the only byproduct.

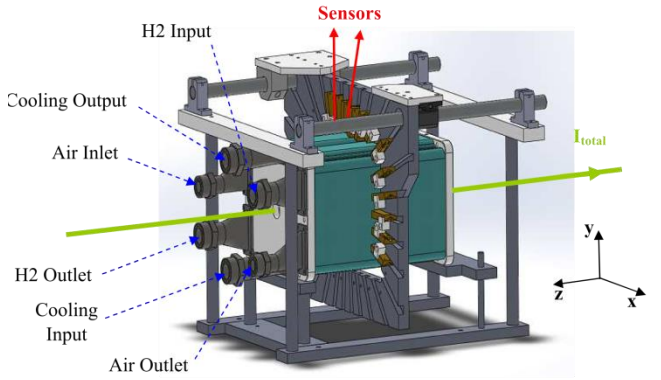

Fig.1. The GENEPAC stack and the magnetic sensors (Le-Ny, 2012)

The stack is made up of 40 cells (area 220 cm²). In this study, a magnetic sensors network previously developed for a diagnosis study (Le-Ny, 2012) is used. Magnetic sensors (Number of sensors Nbs=30) are placed on a perpendicularly plan to the main axis of the stack (Fig.1). 1D fluxgate magnetic sensors are used. Orientations and positions of sensors are defined in a way to eliminate the magnetic field generated by the homogeneous current in the stack. Thus, the measurement is zero when there is homogeneous current density distribution and non-zero in the case of nonhomogeneous current density distribution. The nominal operating conditions of the stack are presented in table. 1.

Table 1. Nominal operating conditions of the stack

Current	110 A
Current density	0.5 A/cm²
Relative humidity (air and H_2)	50 %
Gas pressure	1.5 bar
Air/H_2 stoichiometric ratio	2.2 / 1.5
Fuel cell stack temperature	80 °C

2.2 Magnetic field and current density distribution relation

This work uses the usual relation between the magnetic field and the current density at each time defined by the Biot-Savart law (Durand, 1968):

$$\mathbf{B}(\mathbf{r}) = \int \mathbf{G}(\mathbf{r},\mathbf{r}') \wedge \mathbf{j}(\mathbf{r}') d\mathbf{r}' \qquad (1)$$

with $\mathbf{G}(\mathbf{r},\mathbf{r}') = \frac{\mu_0}{4\pi} \frac{(\mathbf{r}'-\mathbf{r})}{|\mathbf{r}'-\mathbf{r}|^3}$

where **B** is the magnetic field (magnetic flux density) at the position r from the axes origin, **j** is the current density at the position r', μ0 is the permeability of vacuum and G the Green function.

The current density distribution may be different for each cell. For a fuel cells' stack configuration of the current density distributions, stack dimension and sensors positions, the equation (1) gives the magnetic field at the locations of the 30 sensors (Fig. 1).

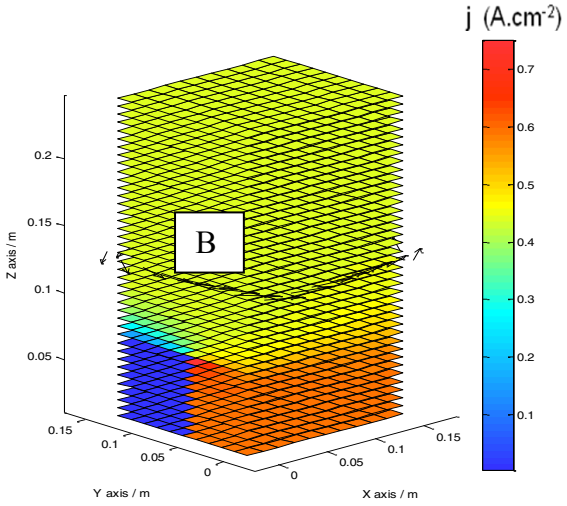

Fig. 2. Magnetic field (arrows) generated by the GENEPAC stack for a given current density distribution

Fig. 2 shows the simulation results for a considered current density distribution in the stack. The colours represent the current density values. The axis scales (x, y,z) represent the real GENEPAC stack dimensions. At the middle of the stack, the arrows show the magnetic field generated by the current distribution in the stack.

2.3 Baselines generation

In the galvanostatic mode, the total current of the stack is constant. A constant current density must get through each cell: so if the current density decreases in some areas, it increases in other areas of the cell, creating nonhomogeneous distribution in the cell. The current density distribution along the fuel cells stack is considered as a distributed variable which is very difficult to manage. We assume that the current density distribution can be discretised into a manageable number of regions. The fuel cell area is divided into four regions (Fig. 3). Region 1 (R1) corresponds to the H_2 outlet of the stack; region 2 (R2) to the air outlet; region 3 (R3) to the H2 inlet and region 4 (R4) to the air inlet (Fig. 1).

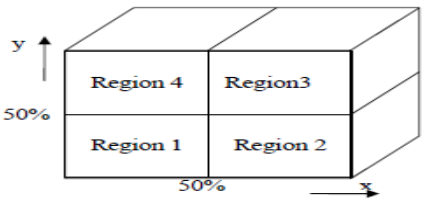

Fig. 3. Stack regions

Due to the linearity properties of magnetic fields, the magnetic field data are proportional to the amplitude of the heterogeneity of the current density. Two values of current density are considered: low current density and high current density. The baselines are columns vectors which contain magnetic fields data. The baselines are generated by mixing regions with low and high current density. Three kinds of

baselines are thus defined: the first kind includes one region with low density current, and the other one with high current density distribution (table2). The second kind includes two neighbour regions with low density current (table3). The third kind includes three regions with low current density (table4).

L: Low current density, H: High current density

Table 2. Baselines 1 to 4

Baseline Number	R1	R2	R3	R4
1	L	H	H	H
2	H	L	H	H
3	H	H	L	H
4	H	H	H	L

Table 3. Baselines 5 to 8

Baseline Number	R1	R2	R3	R4
5	L	H	H	L
6	H	L	L	H
7	L	L	H	H
8	H	H	L	L

Table 4. Baselines 9 to12

Baseline Number	R1	R2	R3	R4
9	H	L	L	L
10	L	H	L	L
11	L	L	H	L
12	L	L	L	H

Thus, baselines vectors ($X(j) \in \Re^{Nbs}$) are defined:

$$X(j) = [MagSens1 \ldots MagSens\ i \ldots MagSensNbs]^T \quad (2)$$

With j=1: N, N=12 is the number of baselines, and MagSens i the magnetic field observed from the ith magnetic sensor.

These baselines do not represent necessarily the faults signatures that have to be detected and diagnosed on fuel cell stack, but they really characterize the current density distributions. To obtain the baseline signature corresponding to each case, data are normalized:

$$\overline{X(j)} = \frac{X(j)}{\|X(j)\|_\infty}, \ j=1: N \quad (3)$$

with $\|X(j)\|_\infty = \max |X(j)_i|_{i=1}^{Nbs}$, i=1: Nbs

And thus:

$$\overline{X(j)} \in [-1 \quad 1]^{Nbs} \quad (4)$$

2.4 Diagnosis method

The proposed fault diagnosis method is mainly based on standard Faults Detection and Isolation (FDI) methodology of model-based diagnosis (Isermann, 2005) as shown in Fig.4. The diagnosis method relies on three steps: residuals generation, residuals evaluation and decision.

The residuals are obtained by comparing the references to the measurements. In a standard FDI methodology, the references correspond to the outputs of the system model under the same operating conditions. In our approach, a baseline matrix (5) characterizing the abnormal behaviour of the system is used as if it was the output of a diagnostic model and where each column represents a reference baseline. No considerations on operating conditions are needed:

$$Mbaseline = \left[\overline{X(1)} \quad \ldots \quad \overline{X(j)} \quad \ldots \quad \overline{X(N)}\right]_{Nbs\ x\ N} \quad (5)$$

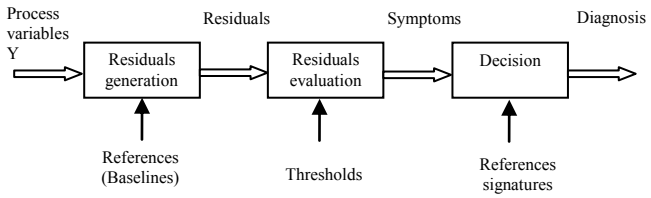

Fig. 4. Diagnosis method principle

The measurements are acquired with a magnetic sensor network and stored in a column vector Y.

$$Y = [Sens1 \ldots Sensi \ldots SensNbs]^T \quad (6)$$

Then, the magnetic fields data are normalized:

$$\overline{Y} = \frac{Y}{\|Y\|_\infty} \quad \text{with } \|Y\|_\infty = max\ |Y_i|_{i=1}^{Nbs} \quad (7)$$

The normalized measurements $\overline{Y}$ are compared to the baselines. Then, the residuals matrix is obtained:

$$Mresiduals = \left[\overline{X(1)} - \overline{Y} \quad . \quad \overline{X(j)} - \overline{Y} \quad . \quad \overline{X(N)} - \overline{Y}\right]_{Nbs\ x\ N} \quad (8)$$

The jth column of Mresiduals is the residual j corresponding to the baseline j:

$$residual(j) = \left[\overline{X(j)} - \overline{Y}\right]_{Nbs\ x\ 1} \quad (9)$$

Commonly the residuals represent the deviation between the system outputs and the predicted process model outputs under the same operating conditions. Here, the residuals have to reflect the closeness of the measurements (magnetic fields data) to the baselines which are used as the output of the diagnostic model.

Then, the residuals have to be evaluated to produce symptoms. A fixed threshold has been used for the residuals evaluation process. The choice of this threshold value (τ=0.2) is based on simulation of model (1), so that the Nbs measurements stay in the inner envelop as shown in Fig. 5 even if the areas predefined in Fig. 3 change from 30% to 200%. Fig. 5 corresponds to the case in which the Nbs measurements stay in the inner envelop even if the area of the first baseline (region 1) is changed from 30% to 200% of the predefined area in Fig. 3.

If an element i of a residual j belong to [$-\tau$ $+\tau$], then it is replaced by 1, otherwise, it is replaced by 0:

$$Mresiduals\ \lceil i, j \rceil = \begin{cases} 1\ if & |Mresiduals\ [i, j]| \le \tau \\ 0\ if & |Mresiduals\ [i, j]| \ge \tau \end{cases} \quad (10)$$

Then the matrix will be a combination of 0 and 1, and symptoms are obtained by summation of columns elements:

$$Symptom_j = \sum_{i=1}^{Nbs} Mresiduals\ [i, j] \quad for\ j = 1 : N \quad (11)$$

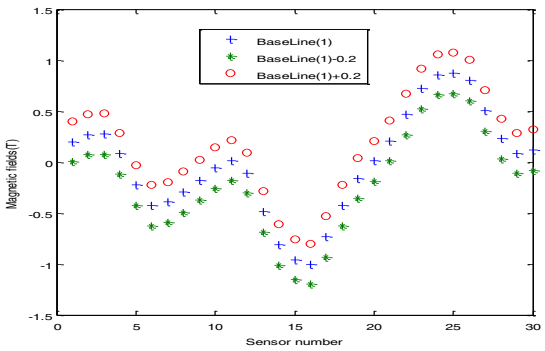

Fig. 5: Residual evaluation

The symptoms j are indicators of the presence of low current density on the regions corresponding to the baseline j.

The last step of the diagnosis method (Fig 4) focuses on the decision step. This is done by classifying the symptoms.

With the threshold value considered, in the case of the presence of three different current densities on the stack section, the value of the symptom j (only for j=1 to 4) is greater than 9 when the low current area is at least 100% of the predefined area of the baselines j (Fig. 3). Only symptoms greater than 8 are taken into account.

To create classes (12), some qualitative variables are defined: G: Baseline which have global heterogeneity (three regions); Half: which have half heterogeneity (two regions); High: Baseline which have high area heterogeneity (one region).

$$G = Baseline \left(k : \max_k \left(symptom_k \Big|_{k=9}^{k=12}\right)\right)$$
$$Half = Baseline \left(k : \max_k \left(symptom_k \Big|_{k=5}^{k=8}\right)\right) \quad (12)$$
$$High = Baseline \left(k : \max_k \left(symptom_k \Big|_{k=1}^{k=4}\right)\right)$$

Each variable may take 4 values if at least one symptom is greater than 8 otherwise it takes the value zero. Thus, there are 5^3 cases to distinguish, which defines 125 different classes. The decision is done by calculating these qualitative variables and comparing them to the reference classes.

Another indicator D (dominant heterogeneity) that depends on the others defined above may be defined to extract the baseline that has highest symptom:

$$D = \text{Baseline} \left(k : \max_k \left(\text{symptom}_k \Big|_{k=1}^{k=12}\right)\right) \quad (13)$$

D represents the region or regions which has the lowest current density distribution. There are (5^3x3)-14 cases with the added one. In regard to PEM fuel cell system and actuators faults, if each fault and faulty modes belong to one or several of the predefined classes in a distinguishable way, the proposed method becomes a remarkable tool which may be used also in the context of fault detection and isolation.

2.5 An illustrative example

We have assumed that the baselines consider only two levels of current density (high and low). This example demonstrates that the proposed method is available for more complex current densities heterogeneities. Here is an example with three different current heterogeneity values (Fig.6). The arrows correspond to the magnetic field generated by the current distribution in the stack.

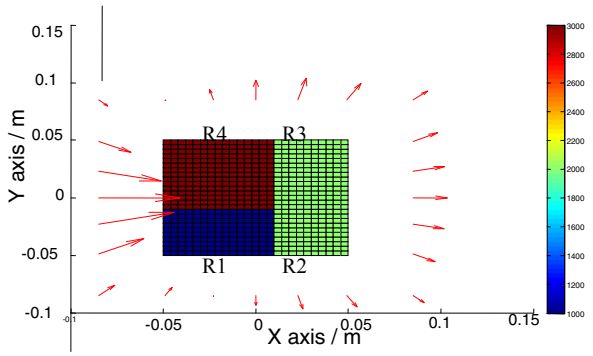

Fig. 6. Current density distribution example

Thus, by applying the method, the calculated symptoms are:

$$Symptoms = [9 \quad 10 \quad 2 \quad 5 \quad 3 \quad 4 \quad 16 \quad 3 \quad 4 \quad 4 \quad 7 \quad 13]$$

With the symptoms vector, for j=9:12, the 12th term is greater than 8, so it corresponds to baseline 12 (L for R1, R2 and R3; H for R4). For j=5:8, the 7th term is greater than 8, so it corresponds to baseline 7 (L for R1, R2; H for R3, R4). For j=1:4, baseline 1 and 2 are greater than 8 (L in R1, L in R2), the highest term greater than 9 is the 2nd one, which corresponds to baseline 2 (region R2). This result may be automatically detected and classified by the proposed classification (Table5).

Table 5. Current density distribution classification

Class	G	Half	High	D
k	12	7	2	7

The tool classifies a given current density distribution and gives us the cartography of low frequency current density distribution within the stack, about the global heterogeneity (3 regions), 2 regions, the high area heterogeneity and the dominant heterogeneity.

3. EXPERIMENTAL RESULTS

In order to test the feasibility of the proposed method, two types of experiments were performed on the GENEPAC stack: performance degradation due to ageing (sixty hours of operation without changing any operating conditions) and actuator fault (change of an operating condition).

The current density distribution at the middle of the stack was measured by a plate inserted between two cells to measure current density (Sociality S + +). This method doesn't give the distribution along the entire stack.

Differential measurements have been used in order to eliminate electromagnetic disturbance (earth field, equipment cables) (14). The differential measurement indicates the change in the current density distribution.

$$B(t0) = B_{earth} + B_{cable} + B(t0)_{stack}$$
$$B(t1) = B_{earth} + B_{cable} + B(t1)_{stack} \quad (14)$$
$$B_{difference} = B(t1) - B(t0) = B(t1)_{stack} - B(t0)_{stack}$$

The diagnosis method may be applied at each instant, but this is not necessary if there is no change in the operation mode. Event based diagnosis would allow us to define the measurements instants with a detection algorithm. This part is not studied in this paper.

3.1 Low air stoichiometric ratio study (actuator fault)

The first test is an actuator fault which is induced by steps decrease of stoichiometric air ratio which promotes flooding of the outlet fuel cell Fig. 7 shows the magnetic field with respect to air stoichiometric ratio steps. The instant t0 corresponds to the stack operation under the nominal operating conditions of the stack (Table 1)

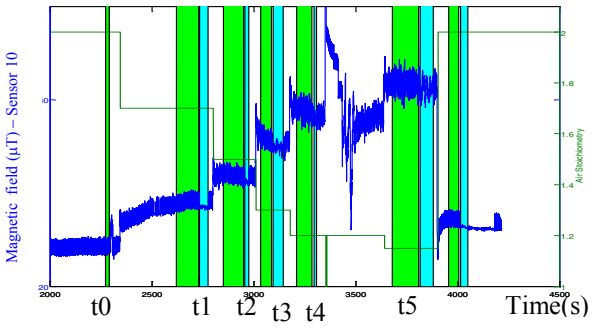

Fig. 7. Air stoichiometric ratio steps and magnetic field measurements on one sensor (10)

Table 6. Symptoms for low air stoichiometric ratio

j	1	2	3	4	5	6	7	8	9	10	11	12
Δt1	7	11	12	4	6	22	3	2	9	3	2	14
Δt2	8	11	10	2	3	22	3	2	9	2	3	15
Δt3	7	13	9	2	2	23	2	3	7	3	3	15
Δt4	8	11	7	2	3	23	2	3	8	3	3	15
Δt5	8	12	7	2	3	21	3	2	7	3	3	15

Table 6 represents the symptoms obtained by applying our method using the differential measurements. With the symptoms vector, for j=9:12, the 9th and 12th terms are greater than 8, which corresponds to baseline 9 and 12. For j=5:8, the 6th term is greater than 8, so it correspond to baseline 6. For j=1:4, the highest terms greater than 9 are the 2nd one and the 3rd one for the 3 first rows, which correspond to baseline 2 and 3.

The global heterogeneity corresponds to baseline 12 (L for R1, R2 and R3; H for R4). Thus, half heterogeneity has theoretically three possibilities: baseline 6 or baseline 7 or zero value, which induce that the high area may be baseline 1 or baseline 2 or baseline 3 or zero value. The measurements of the studied case belong to the classes listed in Table 7. Here the half heterogeneity is baseline 6 so the measurements belong to class 2 only at t1. After t1 all the measurements belong to class 1. This fault can be detected by the two classes; at the beginning with class2 and after severe fault with class 1.

Table 7. Low air stoichiometric ratio classification

Class	G	Half	High	D
1	12	6	2	6
2	12	6	3	6

Fig.8 shows the current density distribution evolution between t5 and t0 measured with the invasive method (S++ card). We observe that the current density tends to concentrate towards the oxygen input (R4) and with low level towards the hydrogen output (R1). We can see also that the output oxygen region (R2) produces lower current density than the other regions. Thus, effectively our method gives the same cartography.

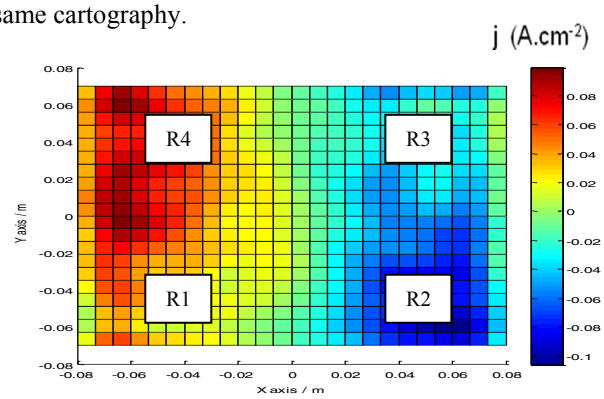

Fig.8. Current density measurements with S++ device between t5 and t0 (Δt5)

3.2 Performance degradation monitoring

The following experiment illustrates the degradation monitoring of stack during sixty-one hours under the nominal operating conditions of the stack (Table 1). The magnetic field is represented with respect to voltage deviation on the cell number 20 in Fig. 9. The magnetic field is again correlated to the performance degradation (voltage decrease). The measurements instants at which the method is applied are: [t0, t1, t2, t3] = [0.3h, 28h, 42h, 61h].

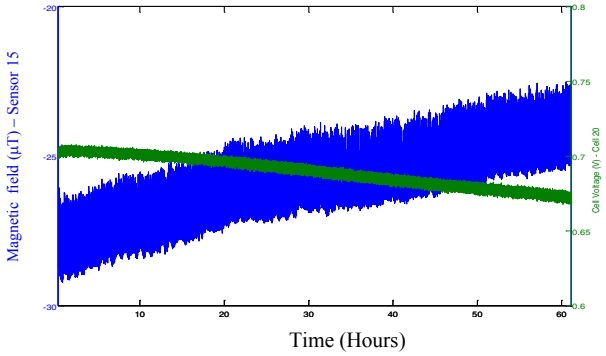

Fig. 9. Cell voltage and magnetic field on one sensor (15)

Table 8 represents the symptoms obtained by applying the proposed method. For j=9:12, the 9th and eventually 12th terms are greater than 8, which corresponds to baseline 9 and 12. For j=5:8, the 6th term becomes greater than 8 at time t2, and the 8th at time t3. For j=1:4, the symptom greater than 8 is at time t1 for j=3. This shows that the current density start to decrease in R3 and spreads with time through the other regions (R2 and R3). But do not increase for (R3 and R4) because there is a part of R4 which produces high current with R1.

Considering classification: the global heterogeneity corresponds to baseline 9 (L for R2, R3 and R4; H for R1), so theoretically, half heterogeneity may be baseline 6 (L for R2

and R3) or baseline 8 (L for R3 and R4) or zero value, then the high area may be baseline 2 or baseline 3 or baseline 4 or zero value.

Table 8. Symptoms for performance degradations

j	1	2	3	4	5	6	7	8	9	10	11	12
Δt1	4	8	14	9	3	8	4	5	17	5	2	10
Δt2	4	6	8	8	2	10	4	7	16	7	3	7
Δt3	4	7	6	6	2	12	3	9	20	3	3	6

At t1, the high heterogeneity is baseline 3 and the half heterogeneity has zero value so the measurements belong to class 4 in Table 9 (beginning of performance degradation). After this, the half heterogeneity is activated in baseline 6 and the high heterogeneity has zero value so the measurements belong to class 3. This fault (performance degradation due to long term functioning) can be detected by the two classes.

Table 9. Performance degradation classification

Class	G	Half	High	D
3	9	6	0	9
4	9	0	3	9

Fig. 10 shows the current density distribution evolution between t3 and t0 (sixty hours) measured with the invasive method. It shows the local performance degradation under time. The region (R2 and R3) have lower current density than (R1 and R4), and the current density is low for R3, R2 and a part of R4, high for R1. It corresponds to baseline 6 and baseline 9 respectively. Thus, effectively our method gives the same cartography.

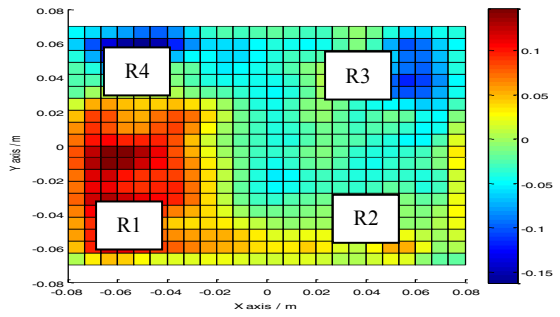

Fig. 10. Current density measurements with S++ device between t3 and t0 (Δt3)

4. CONCLUSION

In this study, we have considered the problem of faults diagnosis in a PEM fuel cell system which is a complex multi scale system. This method provides local information about the current density distribution and signatures corresponding to the faulty modes and faults causes: external causes as the decrease of the air stoichiometric ratio due to an actuator fault (auxiliary components) and internal causes as of the performance degradations due to long term functioning (fuel cell stack). We have shown that the faulty mode can be represented by pattern which should be classified. These results are in concordance with those given by direct current density measurements. This method can be directly included in a fault tolerant control strategy to take compensatory actions to realize uniform current density distribution. In future, the characterization of other faulty scenario will be done as well as the automation of the proposed approach.

Acknowledgements: The authors are grateful to all partners of the OMMNISCIENT program (ANR), especially PSA and the LITEN/CEA for their help and the possibility of using the experimental data performed during the M. Le Ny PhD on GENEPAC stack from PSA.

REFERENCES

Aitouche, A., Q. Yang, B. Ould Bouamama (2011). Fault Detection and Isolation of PEM Fuel Cell System based on Nonlinear Analytical Redundancy: An application via Parity Space Approach, *The European Physical Journal Applied Physics*, **54**(02), 23408-19

Borup, R.; Meyers, J.; Pivovar, B.; Kim, Y.S.; Mukundan, R.; Garland, N.; et al. (2007) Scientific aspects of polymer electrolyte fuel cell durability and degradation. *Chem. Rev*., **107**, 3904–3951.

Chikahisa T., Y. Tabe, Kikuta K., Nohara N. (2009). Measurement of water production phenomena, temperature, and current density distributions in a pomymer electrolyte fuel cell. *Proceedings of the ASME 2009 Conference on Smart Materials, Adaptive Structures and Intelligent Systems SMASIS2009* , September 21-23, Oxnard, California, USA

De Lira. S, Puig, V, Quevedo, J. (2010), Robust LPV model-based sensor fault diagnosis and estimation for a PEM fuel cell system. *Control and fault-tolerant systems Conference* (SysTol), Nice, France, 819 – 824.

Durand E., Tome Magnétostatique, 1968, *Edition MASSON*, Paris, France.

Görgün H., M. Arcak, and F. Barbir.(2005). A voltage-based observer design for membrane water content in PEM fuel cells, *IEEE ACC*, Portland, USA, 4796-4801

Hauer K.H., Potthast R., Wuster T., Stolten D. (2005). Magnetomoghraphy-a new method for analysing fuel cell performance and quality. *J. Power Sources*, **143**, 67-74

Isermann. R (2005). Fault-Diagnosis system systems, an introduction from Fault Detection to Fault Tolerance, *Edition Springer*, Berlin

Le Ny M. (2012). Diagnostic non invasif de piles à combustible par mesure du champ magnétique proche. PhD thesis, Grenoble-INP, France

Rubio M.A., A. Urquia, S. Dormido (2007). Diagnosis of PEM Fuel Cells through Current Interruption. *Journal of Power Sources*, **171**, 670-677.

Schmittinger W., A. Vahidi (2008). A review of the main parameters influencing long-term performance and durability of PEM fuel cells. *J.Power Sources,* **180**, 1-14.

Yousfi Steiner, N., D. Candusso, D. Hissel, P. Moçoteguy (2010). Model-based diagnosis for proton exchange membrane fuel cells Polymer Electrolyte Fuel Cells. *Mathematics and Computers in Simulation*, **81**, 158-170